An Improved Adaptive Coordination Control of Wind Integrated Multi-terminal HVdc System

Yang, Q, Shen, J, Li, J, He, H, Wei, Z & Igic, P

DOI 10.1109/tpel.2022.3228949
ESSN 0885-8993

Publisher: IEEE

An Improved Adaptive Coordination Control of Wind Integrated Multi-terminal HVdc System

Qingqing Yang, *Member, IEEE*, Jun Shen*, Jianwei Li, *Member, IEEE,* Hongwen He, *Senior Member, IEEE*, Zhongbao Wei, *Member, IEEE*, Petar Igic, *Senior Member, IEEE*

***Abstract*—The increasing penetration of the renewables and integration of the power electronic devices leads to lower system inertia, which is changeling the system stability of an MTdc system. This paper presents an improved adaptive predictive control with the multi-objective targets coordinating the key parameters that the dc voltage, ac frequency and power-sharing among the terminals in the multi-terminal HVdc (MTdc) system. Specifically, we contribute two main points to the relevant literature, with the purpose of distinguishing our study from existing ones. First, the proposed method is based on minimal information exchange by only considering neighbouring terminals. Second, the adaptive control is achieved by setting a weighted fitness function to adaptively tune the weights with the effective integration of the trust-region and particle swarm optimization. A four-terminal HVdc system built within the IEEE 30-bus ac system is used as the study case to validate the robustness and efficiency of the proposed method. In the case study regarding the multi-objective fitness function, the proposed approach benefits in suppressing the voltage deviation, providing frequency support and establishing an automatically updated power equilibrium leveraging by the adaptive parameters.**

***Index Terms*—Coordination control, hybrid system, model predictive control, particle swarm optimisation, wind generation.**

I. Introduction

With the advancement of intensive high-capacity dc transmission projects and the development of large-scale wind farms, some areas with clean energy enrichment have evolved into traditional dc transmission lines and new energy high-permeable power grids [1-3]. Under the multi-dc asynchronous delivery pattern, a large number of converter-interfaced sources of energy, such as wind power, continuously replace synchronous generating units, resulting in a significant decrease in system inertia, which may weaken the power grid's ability to resist large-capacity power disturbances [4, 5]. As a result, a major concern has been raised about automatically appropriate power-sharing taking into account dc voltage deviation and frequency support [6].

Frequency regulation can be implemented on either side, providing dc voltage regulation for the MTdc system transmitting renewable energy from remote sources, such as a wind farm, to the centre demand area [7-10]. Traditional droop control, on the other hand, has a strong interaction with the droop character, which reduces the efficiency of the control scheme [11]. Furthermore, the grid-side converters will maintain a constant power output until the droop coefficients, which determine the power ratio, are manually changed, implying that traditional droop control will be unable to provide fast frequency support for ac grids [12]. As a result, traditional droop control is incapable of coordinating dc voltage regulation, frequency support, and power dispatch. When it comes to frequency support, numerous studies have found that control schemes that provide frequency support have a very positive impact [13-16]. Paper [17] uses pilot voltage droop (PVD) control to enhance the dc voltage regulation and frequency deviation sharing. However, apart from general dc regulation and frequency support, automatically appropriate power-sharing between MMCs should be taken into account to improve the dynamic response of the whole system. The droop gains are identified with the limits defined for dc-side power-sharing and dc voltage in power-voltage droop control through two energy-based control approaches [18]. The adaptive droop control is proposed to regulate dc voltage considering power-sharing in paper [19]. The virtual synchronous generator (VSG) is another technique that has been applied to allow the MTdc system to operate in the same manner as a synchronous generator (SG) for frequency support and power transfer capability [20, 21]. However, few papers include multi-objective targets that include all key parameters such as dc voltage, ac frequency, and power-sharing among terminals.

The model predictive control (MPC), also known as the receding horizon control (RHC), is a type of model-based control theory that employs linear or nonlinear process models to achieve control goals [11]. The effects of wind-farm side active power output on voltage variation are investigated using predictive control for fast and flexible voltage regulation coordinated with active and reactive power from wind generation [22]. Centralized control is used in a point-to-point HVdc system [23]. However, communication delays and failures can make fast communication unreliable, and the centralised approach with multi-agents necessitates significant computational effort [24]. The decentralized model with local systems will provide a better trade-off between optimality performance and computational time. Hence, the distributed control is proposed in many researches [25-30]. The requirement of system topology and parameter tuning will limit computational burden, and distributed MPC may result in poor overall system control performance [27]. A hierarchical fast frequency control incorporated both a centralised and a decentralised strategy has been introduced in paper [31]. The distributed multi-agent system's structure combines decentralized horizontal interaction with centralized vertical control, which not only improves coordination efficiency but also maintains the system's real-time, dynamic, and fault tolerance. However, the solutions of multi-objective targets would be difficult when combining both the centralized and decentralized method.

This paper presents an improved distributed model predictive

Corresponding author: Jun Shen

control for enabling HVdc interconnectors with the increase of renewable energy generators and share of renewables to improve system stability considering multi-objective factors that voltage regulation, frequency support and power-sharing. Because of its simple structure and vast application, PSO was created and is frequently utilised [32]. The Particle Swarm Optimization (PSO) has been proved to be efficient in finding globally optimal solutions and has been prosperously used in different scenarios such as inertial support optimization from variable speed wind turbine [33], PSO-optimized PID controller [34], optimal energy scheduling [35], etc.. The particle swarm optimization algorithm outperforms other algorithms including the genetic algorithm (GA), differential evolution (DA), bee algorithm (BA), and colonial competitive algorithm (CCA) on accuracy and convergence speed [36]. Particles in PSO can update their positions and velocities as the environment changes, meeting the proximity and quality requirements. Particles in PSO can maintain their stable movement while changing their movement mode to adapt to changes in the environment. As a result, particle swarm systems adhere to the principles including proximity, quality, diverse response, stability and adaptability. In addition, the PSO algorithm can easily solve nonlinear equations and then store the optimal values [36]. The antiwindup proportional and integral controller control parameters are tuned offline using an adaptive velocity PSO technique [37]. To adjust the settings of the PID controller optimally, an optimization strategy based on the PSO algorithm is given [38]. The main parameters of an active disturbance rejection control are optimised using an adaptive PSO method [39]. However, compared with the existing application, it is difficult to solve the multi-object (MO) optimization problems. The trust-region (TR) algorithm can solve a multi-objective control problem (MOCP) to guarantee convergence to the best solution for a high-dimensional problem [40]. Each target function can be optimised independently in multi-object optimization problems, and then the optimal value for each target can be found [41]. In order to improve the existing controller parameter optimization, the adaptivity is achieved by using weighted fitness function coordinating the weighted based trust-region (WTR) and multi-objective particle swarm optimization (MOPSO) algorithm which has an easy realisation, superior performance and low computational complexity. The hardware-in-the-loop (HIL) test system is built including a 4-terminal MTdc system within the IEEE 30-bus network to verify the proposed control algorithm at an experimental level. The key contributions of this paper are:

- Using varying weighted fitness functions, an improved adaptive predictive control with multi-objective targets coordinating key parameters such as dc voltage, ac frequency, and power-sharing among terminals is proposed.
- The implementation of multi-objective targets is based on minimal information interchange coordinating the information only between neighbouring junctions rather than global information.
- The integration of the WTR and the MOPSO algorithm ensure the optimality of the weights to adaptively identify the mismatch between terminals.

The rest of the paper is organised as follows. Section II gives an overview of the control method for the MMC-MTdc system. Section III introduces the adaptive control based on WTR and MOPSO algorithm. Section IV introduces the system modelling on a 4-terminal dc grid interconnecting two synchronous ac areas and two offshore wind farms in the IEEE 30-bus ac system, and the real-time experimental results are presented and discussed. Concluding remarks are given in Section V.

II. Overview of The Proposed predictive control

A. System description

A four-terminal HVdc system is tested in this paper, including two offshore MMCs connected to the wind farms and two onshore MMCs connected to the ac grid. The permanent magnet synchronous generator (PMSG) is used in wind turbines in the offshore wind farm. The real-time grid phase angle is measured on the phase-locked loop (PLL). The dynamics of a wind farm-side MMC can be found from paper [42].

The fluctuating characteristics of wind power will have an adverse effect on grid frequency transient stability, the most noticeable being a deterioration in frequency transient stability capability caused by a lack of inertia. In the traditional VSC-MTdc control mode, the ac frequency on the wind farm side is decoupled from the grid frequency, and the wind farm cannot sense the grid frequency change, so the grid frequency information needs to be transmitted to the wind farm side. The grid connection of large-scale wind farm groups through VSC-MTdc will reduce the equivalent short-circuit capacity of the grid connection point, and bring about a series of stability problems. At the electromechanical transient scale, the wind farm integrated MTdc system cannot participate in the grid frequency regulation, which deteriorates the transient frequency stability of the grid. Hence, ac frequency is selected as a key parameters in the proposed algorithm to achieve the frequency support for the ac power grid, so as to solve the problem of lack of inertia to a certain extent. In the process of frequency support from the dc system to the ac system, ensuring the stability of the ac side's operating state and the stability of the dc voltage is of great significance to the entire multi-terminal flexible dc transmission system. The maintenance of dc voltage is important in the HVdc system. Hence, the dc voltage is selected as the key factor in the proposed methods. The dc voltage and the ac frequency of the ac system are linearly coupled. The dc voltage is adjusted according to the change of the frequency, and the output power of the wind farm is adjusted with the change of the voltage. The disadvantage of this control strategy is that the coefficient of the dc voltage and frequency is a fixed value, the influence of the coefficient between dc voltage and ac frequency on the output power of the wind farm needs to be further considered. Hence, the power is selected as another key factor.

When power disturbance occurs in the system, the dc voltage will change accordingly, and each converter station will adjust to reach a new stable operating point. The new steady-state

operating point should ensure the stability of dc voltage and the balance of active power and provide seemly frequency support to necessarily meet the requirements of optimal operation of the system. Hence, a novel distributed model predictive control is proposed in this paper.

B. The predictive control formulation

Using predictive models integrated with the historical data and future inputs, MPC predicts the future output of the system. Employing a specific performance index, MPC is optimised to obtain feedback correction control in the rolling finite time interval t_i. The feedback including active power from ac grid generation P_g^m, active power on ac grid P_{ac}^m in ac grids, active power from dc grids P_{mmc}^m and dc voltage V_{dc}^m in MTdc system and reactive power Q_{wt}^m in wind generator form a closed loop. The control scheme in each branch is completed through consultation and cooperation between adjacent terminals utilising energy balancing. The adjacent module information will be measured and transferred to the MPC. Since only the first time-step of the control action is executed, a receding rolling horizon manner is operated at the next discrete step $k+1$. Hence, the optimal control will work in the system to withstand the negative influence caused by systematic volatility and faults based on the updated power balance.

The basic principle of MPC is constitutionally the optimisation problem at each sampling time, which explores the control sequence in the finite time domain for optimum performance. The discrete-time state-space model can be expressed:

$$x(k+1) = \mathrm{A}x(k) + Bu(k) \tag{7}$$

where $x(k)$ is the state sequence; $u(k)$ is the control sequence; k is the sampling interval.

The equation can be updated in state-space expression as:

$$\xi(k+1) = \widetilde{\mathrm{A}}x(k) + \widetilde{\mathrm{B}}\Delta u(k) \tag{8}$$

$$\eta(k) = \tilde{\mathrm{C}}\xi(k) \tag{9}$$

where $\Delta u(k) = u(k+1) - u(k)$ is the control increment assuming that $u = \{u(k), u(k+1), \dots, u(k+N-1)\}$; N is the horizon; $\xi(k)$ is the state sequence in prediction horizon; $\eta(k)$ is the output sequence.

The output from the system can be expressed:

$$Y(t) = \Psi\xi(t) + \Theta\Delta\eta(t) \tag{10}$$

where:

$$\xi\left(t+N_p\right) = \widetilde{\mathrm{A}}_t^{N_p}\xi(t|t) + \widetilde{\mathrm{A}}_t^{N_p-1}\widetilde{\mathrm{B}}_t\Delta u(t|t) + \cdots + \widetilde{\mathrm{A}}_t^{N_p-N_c-1}\widetilde{\mathrm{B}}_t\Delta u(t+N_c|t) \tag{11}$$

$$\eta\left(t+N_p\middle|t\right) = \tilde{\mathrm{C}}_{t,t}\widetilde{\mathrm{A}}_{t,t}^{N_p}\xi(t|t) + \tilde{\mathrm{C}}_t\widetilde{\mathrm{A}}_t^{N_p-1}\widetilde{\mathrm{B}}_t\Delta u(t|t) + \cdots + \tilde{\mathrm{C}}_t\widetilde{\mathrm{A}}_t^{N_p-N_c-1}\widetilde{\mathrm{B}}_t\Delta u(t+N_c|t) \tag{12}$$

where N_p is the prediction horizon; N_c is the control horizon.

In general condition, $N_p \geq N_c$. In this paper, $N_p = N_c$ is used for better computational process unless the controller needs to exceed the control horizon [43].

The voltage deviations are expected to be corrected in wind farm side MMC. Hence, the incremental predictive model of the WFVSC can be introduced in eq. (13) by defining the voltage deviations $\Delta V_{sd,sq} = V_{sd,sq}(t+1) - V_{sd,sq}(t)$, the voltage reference deviation $\Delta V_{sd,sq}^* = V_{sd,sq}^*(t+1) - V_{sd,sq}(t)$, the voltage reference deviation of the voltage control loop $\Delta V_s^{ref} = V_s^{ref}(t+1) - V_s(t)$, the voltage deviation in the control loop $\Delta V_{sd,sq}^{int} = \left(\Delta V_{sd,sq}^* - \Delta V_{sd,sq}\right)/s$ and the deviation of i_{cd} in inner loop $\Delta i_{cd} = i_{cd}(t+1) - i_{cd}(t)$ in the control loops.

$$\Delta\dot{x}_{wtvsc} = \left[-\frac{1}{\tau_{in}}\Delta V_{sd}^* + \Delta V_{sd}^{int} - \frac{1}{\tau_{in}}K_p^{out}\Delta i_{cd}, -\Delta V_{sd}^{int} + \frac{1}{\tau_{in}}K_p^{out}\Delta i_{cd}, \frac{1}{\tau_{in}}K_i^{out}\Delta i_{cd}, \frac{1}{C_f}\Delta S_d - \frac{1}{\tau_{in}}\Delta i_{cd}\right] \tag{13}$$

where τ_{in} is the time constant; $K_p = L/\tau_{in}$ and $K_i = R/\tau_{in}$ are the selected proportional-integral (PI) parameters; s is the complex variable.

Meanwhile, the control constraints and state constraints are considered, which relies on the time interval. Hence, the system inequality and equality constraints can be expressed by:

$$\text{s.t.}\begin{cases} \mathrm{V}_{dc}^{min}(k+i) \leq V_{dc}(k+i) \leq \mathrm{V}_{dc}^{max}(k+i) \\ \Delta\mathrm{V}_{dc}^{min} \leq V_{dc}(k+i) - V_{dc}(k+i-1) \leq \Delta\mathrm{V}_{dc}^{max} \\ V_{dc}(k+i) = V_{dc}(k+i-1) + \frac{dV_{dc}}{dP_{mmc}}\Delta P_{mmc}(k+i-1) \end{cases} \tag{14}$$

The reactive power is set to be zero in the onshore ac side converter. The smoothen reactive power can be corrected through wind turbines that the predictive model can be expressed by:

$$\Delta\dot{x}_{wt} = -\frac{1}{\tau_{wt}}\Delta Q_{wt}^{max} + \frac{1}{\tau_{wt}}\Delta Q_{wt}^{ref} \tag{15}$$

$$\text{s.t.}\begin{cases} Q_{wt}^{min}(k+i) \leq Q_{wt}(k+i) \leq Q_{wt}^{max}(k+i) \\ \Delta Q_{wt}^{min} \leq Q_{wt}(k+i) - Q_{wt}(k+i-1) \leq \Delta Q_{wt}^{max} \\ Q_{wt}(k+i) = Q_{wt}(k+i-1) + \frac{dQ_{wt}}{dP_g}\frac{dP_g}{dP_g^{ref}}\Delta P_g^{ref}(k+i-1) \end{cases} \tag{16}$$

where τ_{wt} is the time constant; $\Delta Q_{wt}^{ref} = Q_{wt}(t+1) - Q_{wt}(t)$ is the deviation of the reactive power reference value; $\Delta Q_{wt} = \frac{1}{s\tau_{wt}}\Delta Q_{wt}^{ref}$ is the dynamic behaviour of Q-loop; $\Delta Q_{wt}^{max} = \sqrt{S_{wt}^2 - P_{wt}^2}$ is the available reactive power.

The active power can be updated through MMCs considering the power balancing.

$$\Delta\dot{x}_g = -\frac{1}{\tau_{g\sigma gfn}}\Delta P_g^{max} + \frac{1}{\tau_g}\Delta P_g^{ref} \tag{17}$$

$$\text{s.t.}\begin{cases} P_g^{min}(k+i) \leq P_g(k+i) \leq P_g^{max}(k+i) \\ \Delta P_g^{min} \leq P_g(k+i) - P_g(k+i-1) \leq \Delta P_g^{max} \\ P_g(k+i) = P_g(k+i-1) + \frac{dP_g}{dP_{gmmc}}\frac{dP_{gmmc}}{dP_{gmmc}^{ref}}\Delta P_g^{ref}(k+i-1) \\ \sum_{n=1}^{m}\left[P_{gn}(k+i) - P_{gn}(k+i-1)\right] = 0 \end{cases} \tag{18}$$

where τ_g is the time constant; $\Delta P_g^{ref} = P_g(t+1) - P_g(t)$ is the deviation of the reactive power reference value; $\Delta P_g = \frac{1}{s\tau_g}\Delta P_g^{ref}$ is the dynamic behaviour; ΔP_{gvsc}^{max} is the available active power. The expression of P_g can be replaced by P_{ac} and P_{mmc} for the active power of ac-side and MMC.

The frequency deviation can be illustrated as:

$$\Delta\dot{x}_f = -\frac{1}{4\pi f_{nJ}}\left(D_g + D_l P_g^{ref}\right)\Delta\mathrm{f} + \frac{1}{4\pi f_{nJ}}\left(\Delta P_g^{ref} - \Delta P_{dc}^{ref}\right) \tag{19}$$

$$\dot{f}^{min} \leq f - f_n \leq \dot{f}^{max} \tag{20}$$

where D_g is the damping of the generator; D_l is the damping of the load; J is the inertia; $\Delta f = f - f_n$ is the frequency deviation.

In order to study the dynamic performance on multi-objective, the joint function is studied, which is of interest for droop design purpose.

$$J = min\omega_1 \sum_{i=1}^{c}\left[\Delta P_{ac}^{ref}(k+i)\right]^T\left[\Delta P_{ac}^{ref}(k+i)\right] + \omega_2 \sum_{i=1}^{c}\left[\Delta P_g(k+i)\right]^T\left[\Delta P_g(k+i)\right] + \omega_3 \sum_{i=1}^{c}\left[\Delta P_{mmc}^{ref}(k+i)\right]^T\left[\Delta P_{mmc}^{ref}(k+i)\right] + \omega_4 \sum_{i=1}^{c}\left[\Delta Q_{wt}^{ref}(k+i)\right]^T\left[\Delta Q_{wt}^{ref}(k+i)\right] + \omega_5 \sum_{i=1}^{c}\left[\Delta V_{dc}^{ref}(k+i)\right]^T\left[\Delta V_{dc}^{ref}(k+i)\right] + \omega_6 \sum_{i=1}^{c}[\Delta f(k+i)]^T[\Delta f(k+i)] + \omega_7 \sum_{j=1}^{n} a_{ij}\left(\frac{P_{mmci}(t)}{\mathcal{P}_i} - \frac{P_{mmcj}(t)}{\mathcal{P}_j}\right) \quad (21)$$

where ω_1, ω_2, ω_3, ω_4, ω_5, ω_6, and ω_7 are the varying weights respectively responding to the ac-side active power deviation ΔP_{ac}, the ac-side synchronous generator power deviation ΔP_g, the converter side power deviation ΔP_{mmc}, the wind farm side reactive power compensation error $\mathcal{E}_{\Delta Q_{wt}}$, the dc voltage regulating error $\mathcal{E}_{\Delta V_{dc}}$, the frequency correction $\mathcal{E}_{\Delta f}$, and the power-sharing error $\mathcal{E}_{\Delta P}$ between local and adjacent MMCs, $\mathcal{P}_i$ and $\mathcal{P}_j$ are the power-sharing ratio.

The power-sharing ratio is measured to ensure the shared power within the limit. If there is no need for power-sharing, the coefficient factor will be set to the pre-set value. If the system requires a share of power, the constraints will be selected in the control scheme. If there is no space for extra power, the presupposed power will be set to a constant.

III. The Adaptive Control Coordinating with WTR and MOPSO Algorithm

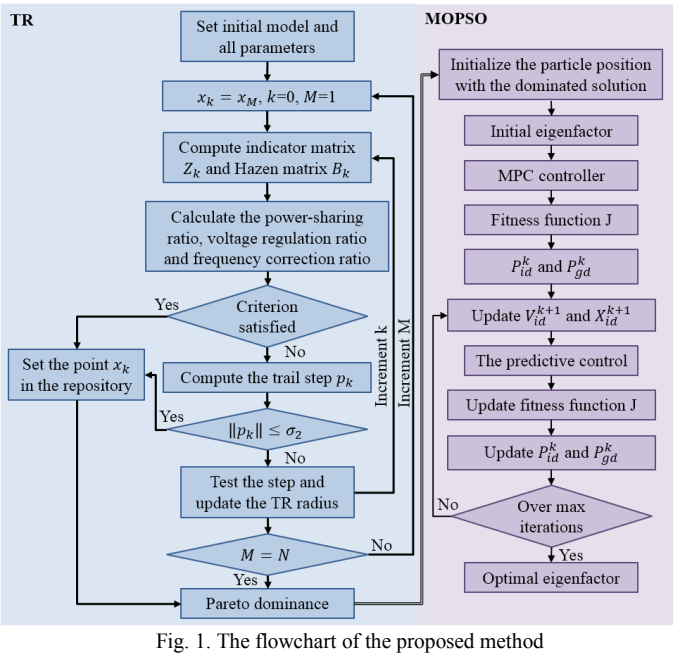

Fig. 1. The flowchart of the proposed method

With varying weights, WTR and MOPSO algorithms are coordinated with the proposed MPC to achieve flexible adaptive control to meet operation requirements. The weights can be automatically obtained by coordinating the WTR and MOPSO algorithms yields trajectories close to the global optimum while only having finite horizon information. The overall structure of the adaptive control strategy is visualized in the flowchart in Fig. 1.

A. The weighted trust-region algorithm

In each iteration of the trust-region algorithm, a trust-region radius is first determined, and within this radius, the minimum value of the second-order approximation of the objective function is calculated. If the minimum reduces the objective function sufficiently, then the next iteration is entered, and the trust-region radius is expanded. If the minimum does not reduce the objective function sufficiently, it indicates that the second-order approximation in the current trust region is not reliable enough, so the trust-region radius needs to be reduced, and the minimum is recalculated. And so on, until the necessary conditions for convergence are met. The error back propagation algorithm uses the error between the sample label information and the actual classification result to construct the loss function between the error energy and the weight. The partial derivative of the weight is obtained through the error energy, combined with the weight gradient descent algorithm, to realize the adjustment of the weight.

The Lagrangian function regarding the fitness function can be defined as:

$$L(x_k, \lambda_k) = f(x_k) + \lambda_k^T h(x_k) \quad (22)$$

where $\lambda_k \in \mathbb{R}$ is the Lagrange multiplier vector related to equality constraint $h(x_k) \in \mathbb{R}$.

The augmented Lagrangian is expressed as [44]:

$$\phi(\mathrm{x}, \lambda; r) = L(\mathrm{x}, \lambda) + r\|h(x_k)\|^2 \quad (23)$$

where r is the penalty parameter.

The initial state is set to be x_k of the k[th] iteration. Taking the x_k as the centre of the circle and making a circle according to the trust-region radius Δ_k, a trust-region is obtained. The second-order approximation of the objective function is made at x_k to get the second-order function after approximation.

$$m_k(p) = f_k + \nabla f_k^T p_k + \frac{1}{2} B_k p_k \quad (24)$$

where f is the objective function; B_k is the approximate Hazen matrix of x_k; $p_k = p_k^n + Z_k \bar{p}_k^t$ is the trail step, which includes two orthogonal components: the normal component p_k^n and the tangential component p_k^t; Z_k is the matrix of the orthonormal basis for the null space ∇f_k^T.

The normal component p_k^n can be obtained by minimizing the TR sub-problem $\frac{1}{2}\|f_k + \nabla f_k^T p_k^n\|^2$, subjecting to $\|p_k^n\| \le \xi\Delta_k$. The tangential component p_k^t can be computed by minimizing $[Z_k^T L(x_k, \lambda_k) + B_k p_k^n]^T \bar{p}_k^t + \frac{1}{2}\bar{p}_k^{t\,T} Z_k^T B_k \bar{p}_k^t$, subjecting to $\|Z_k^T \bar{p}_k^t\| \le \sqrt{\Delta_k^2 - \|p_k^n\|^2}$.

The variable p_k is solved to minimize the second-order function $m_k(p_k)$ in the trust-region. In the trust-region, $m_k(p_k)$ can be found close to the objective function. But they do not come close outside the trust-region. A vector is detected as the trust-region step size that minimizes $m_k(p_k)$ within the trust region. The selection of the trust-region radius is very critical because the iteration will be interrupted if an

unacceptable step size is located with a very large trust-region radius. Hence, the acceptable condition of step size can be expressed as:

$$\rho_k = \frac{f(x_k)-f(x_k+p_k)}{m_k(0)-m_k(p_k)} \tag{25}$$

The augmented Lagrangian function (14) is used as a merit function. The compression is made between the actual reduction $Arep_k$ and the predicted reduction $Prep_k$ which move from x_k to $x_k + p_k$.

$$Arep_k = L(x_k,\lambda_k) - L(x_{k+1},\lambda_{k+1}) + r_k[\|h(x_k)\|^2 - \|h(x_{k+1})\|^2] \tag{26}$$

$$Prep_k = -\nabla_x L(x_k,\lambda_k)^T p_k - \frac{1}{2} p_k^t B_k p_k - \Delta\lambda_k^T(h(x_k) + \nabla h(x_k)^T p_k) + r_k[\|h(x_k)\|^2 - \|h(x_k) + \nabla h(x_k)^T p_k\|^2] \tag{27}$$

The denominator represents the decrease in the quadratic approximation of the objective function, and the numerator is the decrease of the objective function. If ρ_k is on the verge of one, it shows that the quadratic approximation is very close to the objective function, so the step size is acceptable. If ρ_k is close to zero or even less than zero, it shows that there is a big gap between the second-order approximation and the real objective function, so we need to reduce the trust-region radius and recalculate the step size. A threshold is set to be $\sigma \in (0,1)$ to determine the final step. If $\frac{Arep_k}{Prep_k} < \sigma_0$, the radius is decreased to $\sigma_3\|p_k\|$ and the updated trail step is computed using the new radius. If $\frac{Arep_k}{Prep_k} \geq \sigma_2$, the step is an acceptable setting $\Delta_{k+1} = min\{\Delta_{max}, max\{\Delta_{min}, \sigma_1\Delta_k\}\}$. If $\sigma_0 \leq \frac{Arep_k}{Prep_k} < \sigma_2$, the step is an acceptable setting $\Delta_{k+1} = max\{\Delta_{min}, \sigma_1\Delta_k\}$. Hence, the WTR algorithm is terminated on the state either $\|p_k\| \leq \sigma_1$ or $\|Z_k^T\nabla_x L_k\| + \|h_k\| \leq \sigma_2$.

In order to obtain the minimal value of $m_k(p)$, the Cauchy point method is used with a view to decrease the counting amount. The gradient descent direction is fixed to be the direction of p, and then the minimum value is searched in the trust region along this direction. Therefore, the step sized is selected as:

$$p_k^n = -\tau_k \frac{\Delta k}{\|\nabla f_k\|}\nabla f_k \tag{28}$$

$$\tau_k = \begin{cases} 1 & \nabla f_k^T B_k \nabla f_k \leq 0 \\ min(\|\nabla f_k\|^3/\Delta k \nabla f_k^T B_k \nabla f_k, 1) & \nabla f_k^T B_k \nabla f_k > 0 \end{cases} \tag{29}$$

The direction of p_k^n is the same with the gradient descent direction $-\nabla f_k$, and the value is set to be $\tau_k \Delta k$. If $\nabla f_k^T B_k \nabla f_k \leq 0$, $m_k(p)$ is the monotonically decreasing function, hence the step size is set to reach the boundary of the trust-region. Otherwise, $m_k(p)$ is the quadratic function going upwards, then $\nabla m_k(p) = 0$. If the minimum value is within the trust-region, this step size is used. Otherwise, the step size is changed to reach the boundary of the trust region.

B. MOPSO optimisation

In this stage, the particle swarm optimisation is adopted to optimise the performance of the control scheme. The dominated solution obtained from the TR stage is imported to PSO as the initial value. The particle velocity and position can be updated by the eq. (18) and eq. (19).

$$V_{id}^{k+1} = \omega V_{id}^k + c_1 r_1 (P_{id}^k - X_{id}^k) + c_2 r_2 (P_{gd}^k - X_{id}^k) \tag{30}$$

$$X_{id}^{k+1} = X_{id}^k + V_{id}^{k+1} \tag{31}$$

where $V_{id} = (v_1, v, \cdots, v_n)$ is the adjusted particle speed; $X_{id} = (x_1, x_2, \cdots, x_n)$ is the adjusted position; $i = 1,2,3,\cdots,n$; n is the total number of particles in the group; d represents the d-dimensional space; ω is the inertia weight of the previous velocity in the speed calculation in current state; k is the number of iterations; P_{id}^k is local optimal particle position of ith particle, which is also known as P_{best}; P_{gd}^k is global optimal particle position of gth particle, which is the replacement of G_{best}; c_1 and c_2 are the learning factor regarding the influences of the best particles and best global positions in the velocity updating; r_1 and r_2 are the random variables with uniform distribution.

The PSO convergence is based on the fitness function that updates the new velocities and positions of the particles. The PSO algorithm will be affected by the acceleration coefficients c_1 (local learning factor) and c_2 (global learning factor). Based on the test in Fig. 2 that the best performance of the PSO is achieved with an intermediate value that is either too large or too small.

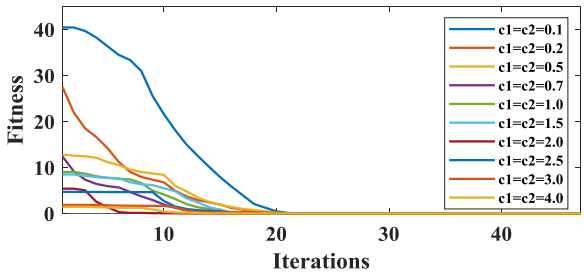

Fig. 2. Fitness iteration diagram of different learning factors c1 and c2.

The inertia weight ω denotes the ability to maintain current velocity can be expressed as:

$$\omega(k) = \omega_{initial} - (\omega_{initial} - \omega_{final})\left(\frac{\mathcal{G}-k}{\mathcal{G}}\right)^m \tag{32}$$

where $\omega_{initial}$ and ω_{final} are the initial and final inertia weight, and $\omega_{initial} > \omega_{final}$; $\mathcal{G}$ is the maximum number of the interactions; m is the nonlinear index.

When inertia weight is more considerable, the ability of global optimum is better. When inertia weight is a smaller value, the method has a better convergence with better local optimisation ability. Hence, the inertia weights are either too large or too small, and $\omega_{initial}$=0.9, ω_{final}=0.4 are selected.

Optimisation of predictive control is not a one-time process but a repeated process with the increase of sampling time hence called rolling horizon. Although the receding horizon method cannot get the comprehensively optimal solution, the deviation of each sampling time is optimised at each sampling instant repeatedly, hence, timely correcting the various tricky situations during the control process. The fitness function can be treated as the multi-objective target that can be achieved stepwise and fractionated through constraints application scenarios.

When dealing with large disturbances and faults, the DC voltage deviation is the most important factor to consider when evaluating the performance of a VSC-MTDC system. The DC voltage deviation is more important for the safe operation of entire MTDC system. The capacitance can be reduced by

reducing the output voltage deviation. As a result, a small voltage deviation is critical for lowering the cost and volume of electrolytic capacitors, the weakest link in power electronic circuits. As a result, the voltage deviation is used to evaluate the performance of proposed method.

IV. System Studies

A. Test system

This section presents the detailed simulation results to validate the effectiveness of the proposed method on a four-terminal HVdc system embedded with the IEEE 30-bus test system, as shown in Fig. 3. The MMC 1 and MMC 2 are connected to the dc network through bus-1 and bus-2 and the ac network through bus-15 and bus-24. The active powers of the converter station are determined by the proposed control, and the reactive powers are set to be zero. The MMC 3 and MMC 4 absorb the powers from two separate wind farms connected to the dc network on bus-3 and bus-4. The power rate in all four terminals is set to be 1000MW. The initial active powers of dc grid MMC 1, 2, 3 and 4 are 449MW, 362MW, 237MW and 619 MW, respectively. Two wind farms are connected through 200 km long dc cables, while the rest of the dc systems are connected through dc overhead lines, which are 150 km, 350 km and 500km long. The ac-side d-axis current reference is 1 A, and q-axis current reference is 223 A, corresponding to 5 MW at a standard voltage. The system is equipped with the superconducting fault current limiters (SFCLs) in the terminal of the dc transmission lines together with the mechanical dc circuit breakers (CBs) forming the protection devices in the system to limit the maximum fault current.

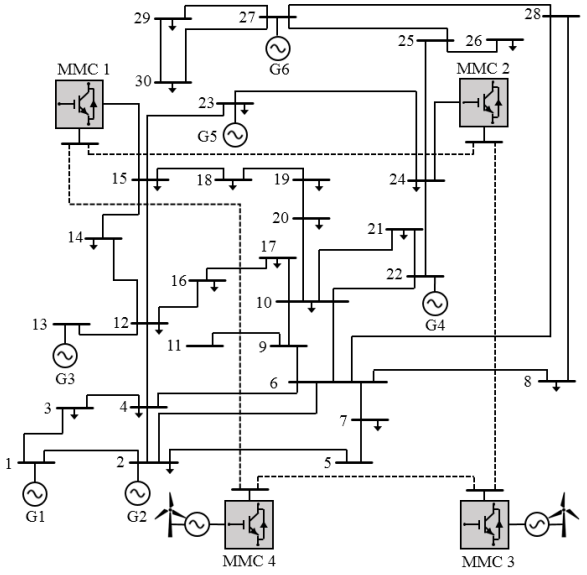

Fig. 3. The four-terminal MTdc system embedded with IEEE 30-bus test system configuration

The detailed MTdc system technical specifications and the tuning and simulation parameter values are specified in Table I and Table II, respectively. All the simulation results are presented in per-unit values.

Table I The detailed parameters of the test system

Specifications	Operating rating
Lcable1; Lcable2; Lcable3; Lcable4	96 mH; 124 mH; 49 mH; 192 mH
Rcable1; Rcable2; Rcable3; Rcable4	2.68 Ω; 1.92 Ω; 0.49 Ω; 2.02 Ω
Ccable1; Ccable2; Ccable3; Ccable4	0.26μF; 0.26μF; 0.48μF; 0.50μF
DC base current	250 A
DC base power	500 MW
Rated power of MMC	1060 MVA
Rated voltage of MMC	230 kV ac; ±400 kV dc
Arm reactor	50 mH
Rated power of WT	10 MVA
Rated voltage of WT	690 V AC
Wind speed; Rotor speed	12 m/s; 10 rpm
Inertia	$151*10^6$ kgm^2
L-filter impedance	(0.01+j0.25) p.u.
Diameter of SFCL	80 mm
Pitch of SFCL coil	15 mm
Tape to tape separation	0.3 mm
Critical current of superconductors	253 A
Line resister	0.011 Ω
Load resister	1 Ω

Table II The parameter in the proposed algorithm

Parameter	Value	Parameter	Value
σ_0	0	N	20-50
σ_1	2	PSO iteration	50-200
σ_2	0.5	w	0.4
σ_3	0.5	c_1	1.3
Δ_0	$(1,1.5)\Delta_{\min}$	c_2	1.3
$\Delta_{\max}$	$10^5\Delta_0$	ε_1	10^{-7}
$\Delta_{\min}$	10^5	ε_2	10^{-7}

B. Hardware in the loop test system

A hardware-in-the-loop test system (Fig. 4), including the real-time simulator RTDS embed with the ODAC and GTDI cards, the analogue interface, the digital interfaces and the DSP (TMS320F28335) is introduced in this paper to test the real-time performance of the proposed method. The RTDS is regarded as a convincing simulator with real-time simulation capability and system flexibility compared with the other traditional simulation method [45]. Due to difficulties of building a real MTdc experiment platform in the laboratory environment, the test case is built and operates in the closed-loop, therefore the effects of the control actions can be observed through real-time interaction with the simulation. The control algorithm is built in an external DSP which will generate the physical control signals to verify the effectiveness and real-time of the proposed methodology at an experimental level.

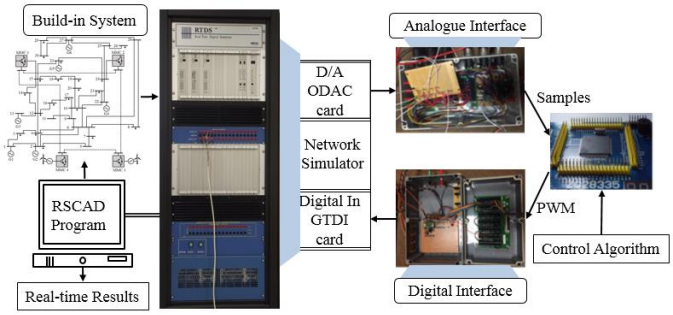

Fig. 4. The RTDS HIL test setup

The four-terminal MTdc system embedded with IEEE 30-bus test system is established and simulated in the RTDS. The control scheme is designed in DSP, which is used to receive the analogue signals from the ODAC card in RTDS and generate the digital control signals through the embedded ADC module. The control signals are processed by a GTDI card built in

RTDS. The analogue signals generated from the ODAC card are at ±10 V, whereas the signal in the DSP peaks at 3.3 V. And the signals from the DSP is at 3.3 V level, whereas the GTDI card has 5 V logic. Hence, analogue and digital interfaces are required in the test system.

C. *Results and discussion*

The proposed method is firstly tested under the line-to-ground fault which occurs at 1 s compared with the centralized MPC method (CMPC). The proposed control scheme is then studied under load changes on the ac-side compared with the traditional droop control. A 200 MW load is decreased on terminal 2 at 2 s.

The initial start of the whole system is studied for all four terminals (T1, T2, T3, and T4), and the active power at the initial start is shown in Fig. 5 compared with the centralized MPC control method. The difference is slight about 0.0001 p.u. between the curves with the proposed method (which is short for Prop) and the centralized MPC method (CMPC), which means these two methods can achieve a good performance at the initial start of the system. Furthermore, the fluctuations of the waveform are reduced by using the proposed method until the system entering stability.

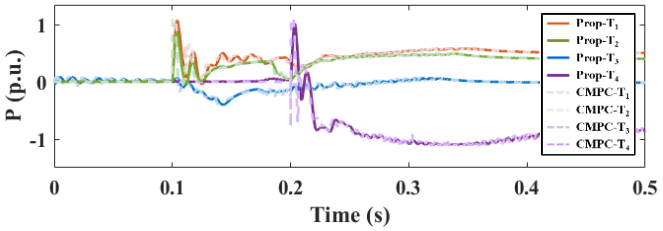

Fig. 5. The active power at the initial start of the system

The proposed method is compared with the centralized control without communication for automatically power-sharing and centralized MPC scheme in Fig. 6 and Fig. 7, respectively. The influence of the proposed method can be found to effectively alleviate the influence of the ac system to the greatest extent. Because a fault occurs on the system, the

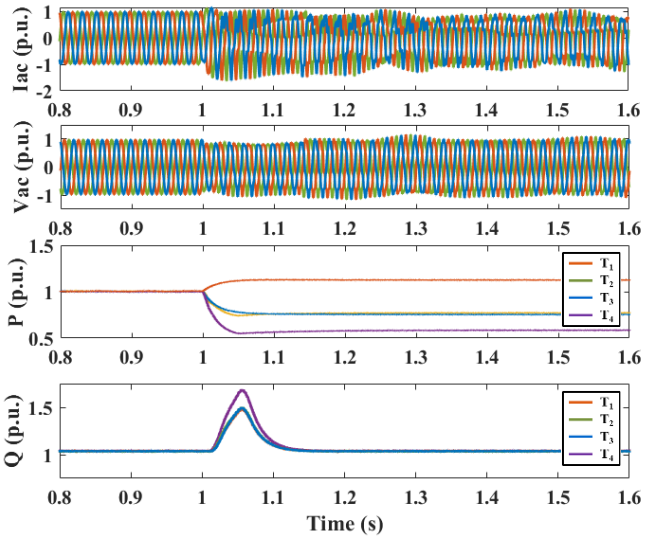

Fig. 6. The performance of ac voltage, ac current, active power and reactive power with non-adaptive control

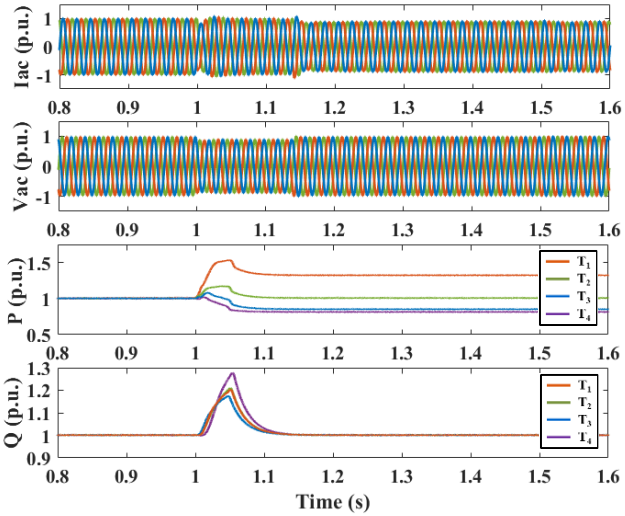

Fig. 7. The performance of ac voltage, ac current, active power and reactive power with the proposed control

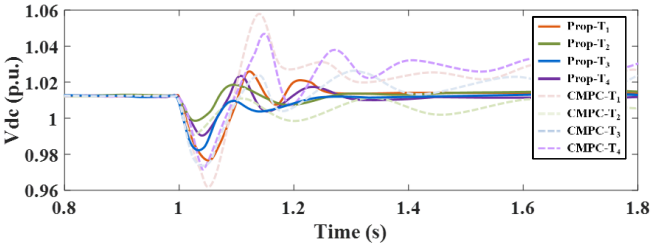

Fig. 8. The performance of dc voltage regulation compared with CMPC

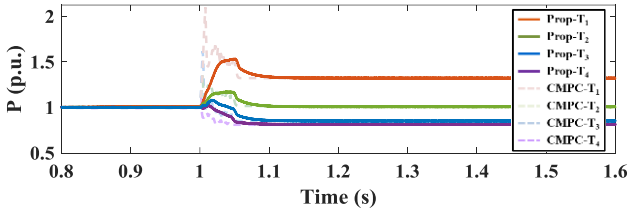

Fig. 9. The performance of active power with power-sharing compared with CMPC

The dc voltage regulation (Fig. 8) is the key function of a control scheme. It can be observed that the voltage deviations are dramatically alleviated, and the voltage is equilibrated quickly after the change of loads. The voltage value can be restored to the nominal value faster using the proposed method. The standard deviations of dc voltage are 0.8358% for centralized MPC control and 0.8012% for the proposed control, respectively. Fig. 9 performs the response from active power on four terminals. It can be observed that the response speed is faster than the centralized method with global searching. Furthermore, the waveforms are shown in a smoother form because of the adaptivity of the proposed control scheme with consideration of active powering sharing.

The results of using the proposed method show the trajectories converge to equilibrium. The proposed distributed prediction control method can reduce the power losses effectively by cutting down the average losses in one time step from 11.9514 MW with MPC to 10.3620 MW with the new method.

Fig. 10 depicts the dc voltage regulation in the second case with load changes. The dc voltage standard deviations for droop control and suggested control are 0.9020% and 0.8109%,

respectively. Fig. 11 performs the response from active power on four terminals. With the improved power balance, the active power can be returned to the steady state in a shorter amount of time.

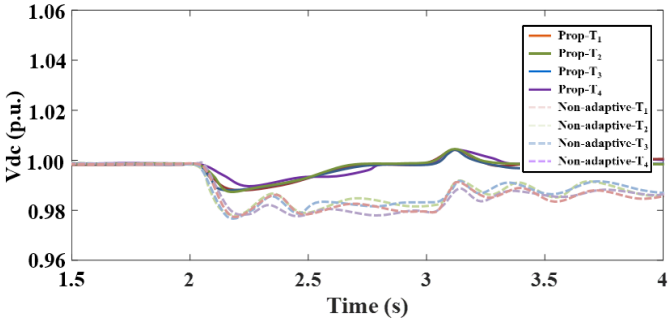

Fig. 10. The performance of dc voltage regulation compared with non-adaptive control

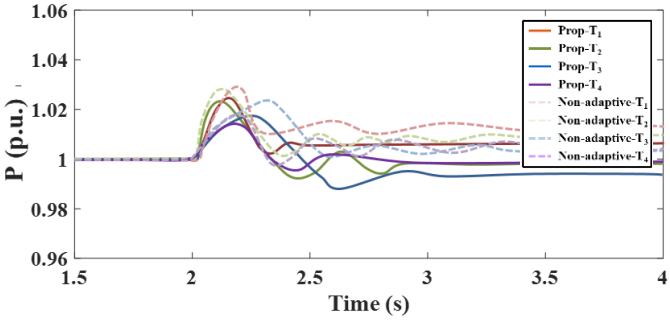

Fig. 11. The performance of active power with power-sharing compared with non-adaptive control

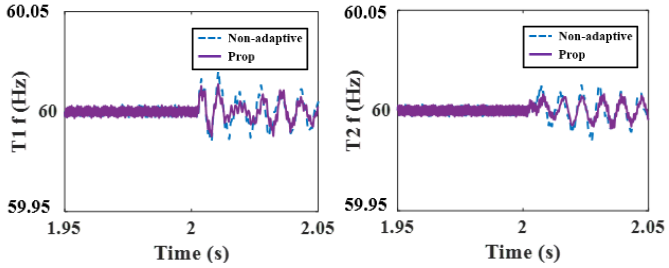

Fig. 12. The performance of ac frequency compared with non-adaptive control

Under the conventional droop control strategy, when the load changes, the converter station cannot respond to the frequency of the ac side system, and neither the dc voltage nor the VSC-MTDC transmission power changes. Active power balance can only be achieved by relying on the frequency regulation of the generator set and the power frequency characteristics of the load. The ac side frequency is tested in Fig. 12. The fluctuation of the frequency changes can be observed with 15.57% improvement.

The proposed method can quickly mitigate fluctuations and bring the system back to a steady state. According to the results of the tests, the proposed method can effectively work in situations where the system is disrupted. First of all, the results show smoother lines at the initial start of the operation. This method will effectively mitigate system fluctuations and quickly return the system to its normal state when there is a sudden change of loads on the ac-side system. Furthermore, the control method can provide the capability to withstand system faults. Meanwhile, if the system requires an update to the new equilibration condition, power-sharing is also considered. Hence, the proposed method is proved to be efficient and robust to retard the voltage and active power deviation, provide a new balance of power-sharing and provide frequency support to ac network. The results of the operation show that this system features excellent robustness and adaptability.

V. Conclusion

This paper proposed an adaptive multi-objective predictive control for the MMC-MTdc system integrated with wind farms to update the equilibrium of the power, regulate the voltage and provide frequency support to the ac system. The adaptive optimisation of the weights using a WTR-MOPSO integrated method is presented. The multi-objective predictive control is proposed to acquire the updated system parameters with analytical constraints considering power-sharing in only two adjacent dc terminals with minimal information required. The adjustable trade-off among voltage regulation, frequency support and power-sharing is considered in the constraints. The proposed control method is verified in a 4-terminal MTdc system integrated with the IEEE 30-bus test ac system using HIL experimental platform. Compared with a non-adaptive predictive control scheme, the effectiveness of limiting the influences from the system deviation and bringing the system back to normal promptly are proved. The power losses are decreased up to 13.30%. The result shows that the control method can adaptively operate under different system conditions in high performance. With the predictability of predictive control, rolling optimisation and feedback correction, the proposed method can better adapt to the actual system and have stronger robustness.

References

[1] Q. Wang, D. Kundur, H. Yuan, Y. Liu, J. Lu, and Z. Ma, "Noise Suppression of Corona Current Measurement From HVdc Transmission Lines," *IEEE Transactions on Instrumentation and Measurement,* vol. 65, no. 2, pp. 264-275, 2016.

[2] C. Zou *et al.*, "Analysis of Resonance Between a VSC-HVDC Converter and the AC Grid," *IEEE Transactions on Power Electronics,* vol. 33, no. 12, pp. 10157-10168, 2018.

[3] H. Xiao, X. Duan, Y. Zhang, T. Lan, and Y. Li, "Analytically Quantifying the Impact of Strength on Commutation Failure in Hybrid Multi-Infeed HVDC Systems," *IEEE Transactions on Power Electronics,* pp. 1-1, 2021.

[4] S. Cao, X. Zhang, W. Xiang, and J. Wen, "A Power Flow Transfer Entropy based AC Fault Detection Method for the MTDC Wind Power Integration System," *IEEE Transactions on Industrial Electronics,* pp. 1-1, 2020.

[5] J. Fang, P. Lin, H. Li, Y. Yang, and Y. Tang, "An Improved Virtual Inertia Control for Three-Phase Voltage Source Converters Connected to a Weak Grid," *IEEE Transactions on Power Electronics,* vol. 34, no. 9, pp. 8660-8670, 2019.

[6] M. N. Ambia, K. Meng, W. Xiao, A. Al-Durra, and Z. Y. Dong, "Adaptive Droop Control of Multi-Terminal HVDC Network for Frequency Regulation and Power Sharing," *IEEE Transactions on Power Systems,* 2021.

[7] F. D. Bianchi and J. L. Domnguez-Garca, "Coordinated frequency control using MT-HVDC grids with wind power plants," *IEEE Transactions on Sustainable Energy,* vol. 7, no. 1, pp. 213-220, 2015.

[8] S. Balasubramaniam, C. E. Ugalde-Loo, J. Liang, and T. Joseph, "Power Flow Management in MTdc Grids Using Series Current Flow Controllers," *IEEE Transactions on Industrial Electronics,* vol. 66, no. 11, pp. 8485-8497, 2019.

[9] J. Sheng *et al.*, "Control Optimization of Modular Multilevel Resonant DC Converters for Wide-Input-Range MVdc to LVdc Applications," *IEEE Transactions on Power Electronics,* vol. 37, no. 5, pp. 5284-5298, 2022.

[10] F. Deng, Q. Yu, Q. Wang, R. Zhu, X. Cai, and Z. Chen, "Suppression of DC-Link Current Ripple for Modular Multilevel Converters Under Phase-Disposition PWM," *IEEE Transactions on Power Electronics,* vol. 35, no. 3, pp. 3310-3324, 2020.

[11] L. Papangelis, M.-S. Debry, P. Panciatici, and T. Van Cutsem, "A receding horizon approach to incorporate frequency support into the AC/DC converters of a multi-terminal DC grid," *Electric Power Systems Research,* vol. 148, pp. 1-9, 2017.

[12] W. Wang, Y. Li, Y. Cao, U. Häger, and C. Rehtanz, "Adaptive Droop Control of VSC-MTDC System for Frequency Support and Power Sharing," *IEEE Transactions on Power Systems,* vol. 33, no. 2, pp. 1264-1274, 2018.

[13] O. Saborío-Romano, A. Bidadfar, J. N. Sakamuri, L. Zeni, G. Ö, and N. A. Cutululis, "Communication-Less Frequency Support From Offshore Wind Farms Connected to HVdc via Diode Rectifiers," *IEEE Transactions on Sustainable Energy,* vol. 12, no. 1, pp. 441-450, 2021.

[14] R. Yang, G. Shi, X. Cai, C. Zhang, G. Li, and J. Liang, "Autonomous Synchronizing and Frequency Response Control of Multi-terminal DC Systems with Wind Farm Integration," *IEEE Transactions on Sustainable Energy,* pp. 1-1, 2020.

[15] M. M. Kabsha and Z. H. Rather, "A New Control Scheme for Fast Frequency Support From HVDC Connected Offshore Wind Farm in Low-Inertia System," *IEEE Transactions on Sustainable Energy,* vol. 11, no. 3, pp. 1829-1837, 2020.

[16] J. Sun, L. Qiu, X. Liu, J. Zhang, J. Ma, and Y. Fang, "Improved Model Predictive Control for Three-Phase Dual-Active-Bridge Converters With a Hybrid Modulation," *IEEE Transactions on Power Electronics,* vol. 37, no. 4, pp. 4050-4064, 2022.

[17] A. Kirakosyan, E. F. El-Saadany, M. S. E. Moursi, and K. A. Hosani, "DC Voltage Regulation and Frequency Support in Pilot Voltage Droop-Controlled Multiterminal HVdc Systems," *IEEE Transactions on Power Delivery,* vol. 33, no. 3, pp. 1153-1164, 2018.

[18] S. D. Tavakoli, E. Sánchez-Sánchez, E. Prieto-Araujo, and O. Gomis-Bellmunt, "DC Voltage Droop Control Design for MMC-Based Multiterminal HVDC Grids," *IEEE Transactions on Power Delivery,* vol. 35, no. 5, pp. 2414-2424, 2020.

[19] Y. Wang, W. Wen, C. Wang, H. Liu, X. Zhan, and X. Xiao, "Adaptive Voltage Droop Method of Multiterminal VSC-HVDC Systems for DC Voltage Deviation and Power Sharing," *IEEE Transactions on Power Delivery,* vol. 34, no. 1, pp. 169-176, 2019.

[20] Y. Cao *et al.*, "A virtual synchronous generator control strategy for VSC-MTDC systems," *IEEE Transactions on Energy Conversion,* vol. 33, no. 2, pp. 750-761, 2017.

[21] A. Asrari, M. Mustafa, M. Ansari, and J. Khazaei, "Impedance Analysis of Virtual Synchronous Generator-Based Vector Controlled Converters for Weak AC Grid Integration," *IEEE Transactions on Sustainable Energy,* vol. 10, no. 3, pp. 1481-1490, 2019.

[22] K. Shivam, J.-C. Tzou, and S.-C. Wu, "A multi-objective predictive energy management strategy for residential grid-connected PV-battery hybrid systems based on machine learning technique," *Energy Conversion and Management,* vol. 237, p. 114103, 2021/06/01/ 2021.

[23] A. Fuchs, M. Imhof, T. Demiray, and M. Morari, "Stabilization of large power systems using VSC–HVDC and model predictive control," *IEEE Transactions on Power Delivery,* vol. 29, no. 1, pp. 480-488, 2013.

[24] A.N. Tar˘au, B. De Schutter, and J. Hellendoorn, "Centralized, decentralized, and distributed model predictive control for route choice in automated baggage handling systems," *Control Engineering and Applied Informatics,* vol. 11-3, no. Special Issue on Distributed Control in Networked Systems, pp. 24–31, 2009.

[25] L. Yang, T. Liu, and D. J. Hill, "Distributed MPC-based frequency control for multi-area power systems with energy storage," *Electric Power Systems Research,* vol. 190, p. 106642, 2020.

[26] L. Tarisciotti, G. L. Calzo, A. Gaeta, P. Zanchetta, F. Valencia, and D. Saez, "A distributed model predictive control strategy for back-to-back converters," *IEEE Transactions on Industrial Electronics,* vol. 63, no. 9, pp. 5867-5878, 2016.

[27] Y. Jia, K. Meng, C. Sun, L. Yuan, and Z. Y. Dong, "Economic-Driven Frequency Regulation in Multi-Terminal HVDC Systems: A Cooperative Distributed Approach," *IEEE Transactions on Power Systems,* vol. 35, no. 3, pp. 2245-2255, 2019.

[28] L. Subramanian, V. Debusschere, H. B. Gooi, and N. Hadjsaid, "A Distributed Model Predictive Control Framework for Grid-friendly Distributed Energy Resources," *IEEE Transactions on Sustainable Energy,* 2020.

[29] A. N. Venkat, I. A. Hiskens, J. B. Rawlings, and S. J. Wright, "Distributed MPC strategies with application to power system automatic generation control," *IEEE transactions on control systems technology,* vol. 16, no. 6, pp. 1192-1206, 2008.

[30] L. Papangelis, M.-S. Debry, T. Prevost, P. Panciatici, and T. Van Cutsem, "Decentralized model predictive control of voltage source converters for AC frequency containment," *International Journal of Electrical Power & Energy Systems,* vol. 98, pp. 342-349, 2018.

[31] O. Stanojev, U. Markovic, P. Aristidou, G. Hug, D. Callaway, and E. Vrettos, "MPC-Based Fast Frequency Control of Voltage Source Converters in Low-Inertia Power Systems," *arXiv,* 2020.

[32] S. Fang, Y. Wang, W. Wang, Y. Chen, and Y. Chen, "Design of Permanent Magnet Synchronous Motor Servo System Based on Improved Particle Swarm Optimization," *IEEE Transactions on Power Electronics,* vol. 37, no. 5, pp. 5833-5846, 2022.

[33] F. Hafiz and A. Abdennour, "Optimal use of kinetic energy for the inertial support from variable speed wind turbines," *Renewable Energy,* vol. 80, pp. 629-643, 2015.

[34] P. M. Namara, R. R. Negenborn, B. D. Schutter, and G. Lightbody, "Optimal Coordination of a Multiple HVDC Link System Using Centralized and Distributed Control," *IEEE Transactions on Control Systems Technology,* vol. 21, no. 2, pp. 302-314, 2013.

[35] M. G. M. Abdolrasol, R. Mohamed, M. A. Hannan, A. Q. Al-Shetwi, M. Mansor, and F. Blaabjerg, "Artificial Neural Network Based Particle Swarm Optimization for Microgrid Optimal Energy Scheduling," *IEEE Transactions on Power Electronics,* vol. 36, no. 11, pp. 12151-12157, 2021.

[36] M. Sadoughi, A. Pourdadashnia, M. Farhadi-Kangarlu, and S. Galvani, "PSO-Optimized SHE-PWM Technique in a Cascaded H-Bridge Multilevel Inverter for Variable Output Voltage Applications," *IEEE Transactions on Power Electronics,* vol. 37, no. 7, pp. 8065-8075, 2022.

[37] W. Xu, M. M. Ismail, Y. Liu, and M. R. Islam, "Parameter Optimization of Adaptive Flux-Weakening Strategy for Permanent-Magnet Synchronous Motor Drives Based on Particle Swarm Algorithm," *IEEE Transactions on Power Electronics,* vol. 34, no. 12, pp. 12128-12140, 2019.

[38] Z. Qi, Q. Shi, and H. Zhang, "Tuning of Digital PID Controllers Using Particle Swarm Optimization Algorithm for a CAN-Based DC Motor Subject to Stochastic Delays," *IEEE Transactions on Industrial Electronics,* vol. 67, no. 7, pp. 5637-5646, 2020.

[39] C. Du, Z. Yin, Y. Zhang, J. Liu, X. Sun, and Y. Zhong, "Research on Active Disturbance Rejection Control With Parameter Autotune Mechanism for Induction Motors Based on Adaptive Particle Swarm Optimization Algorithm With Dynamic Inertia Weight," *IEEE Transactions on Power Electronics,* vol. 34, no. 3, pp. 2841-2855, 2019.

[40] S. Peitz and M. Dellnitz, "A Survey of Recent Trends in Multiobjective Optimal Control—Surrogate Models, Feedback Control and Objective Reduction," vol. 23, no. 2, p. 30, 2018.

[41] D. Wang, D. Tan, and L. Liu, "Particle swarm optimization algorithm: an overview," *Soft Computing,* vol. 22, no. 2, pp. 387-408, 2018.

[42] Y. Deng, Y. Wang, K. H. Teo, and R. G. Harley, "A simplified space vector modulation scheme for multilevel converters," *IEEE Transactions on Power electronics,* vol. 31, no. 3, pp. 1873-1886, 2015.

[43] Y. Guo, H. Gao, H. Xing, Q. Wu, and Z. Lin, "Decentralized coordinated voltage control for vsc-hvdc connected wind farms based on admm," *IEEE Transactions on Sustainable Energy,* vol. 10, no. 2, pp. 800-810, 2018.

[44] M. El-Shorbagy, "Weighted Method Based Trust Region-Particle Swarm Optimization for Multi-Objective Optimization," *American Journal of Applied Mathematics,* vol. 3, no. 3, p. 81, 2015.

[45] J. Li *et al.*, "Design and real-time test of a hybrid energy storage system in the microgrid with the benefit of improving the battery lifetime," *Applied Energy,* vol. 218, pp. 470-478, 5/15/ 2018.